Maximizing the Nondemolition Nature of a Quantum Measurement Via an Adaptive Readout Protocol

Arjen Vaartjes,[1] Rocky Yue Su,[1] Laura A. O'Neill,[1] Paul Steinacker,[1,2] Gauri Goenka,[1] Mark R. van Blankenstein,[1] Xi Yu,[1] Benjamin Wilhelm,[1] Alexander M. Jakob,[3] Fay E. Hudson,[1,2] Kohei M. Itoh,[4] Chih Hwan Yang,[1,2] Andrew S. Dzurak,[1,2] David N. Jamieson,[3] Martin Nurizzo,[1] Danielle Holmes,[1] Arne Laucht,[1,2] and Andrea Morello[1,*]

[1] *School of Electrical Engineering and Telecommunications, UNSW Sydney, Sydney, NSW 2052, Australia*
[2] *Diraq Pty. Ltd., Sydney, NSW, Australia*
[3] *School of Physics, University of Melbourne, Melbourne, VIC 3010, Australia*
[4] *School of Fundamental Science and Technology, Keio University, Kohoku-ku, Yokohama, Japan*

(Received 23 November 2025; revised 9 February 2026; accepted 2 April 2026; published 15 May 2026)

Quantum error correction benefits from high-fidelity, noninvasive measurements for fault-tolerant quantum computing. Deviations from ideal quantum nondemolition (QND) measurements can disturb the encoded information. To address this challenge, we develop a readout protocol for a D-dimensional system that, after a single positive outcome, switches to probing only the $D-1$ remaining subspace. This adaptive switching strategy minimizes measurement-induced errors by relying on negative-result measurement results that do not perturb the Hamiltonian. We apply the protocol on an eight-dimensional ^{123}Sb nuclear qudit in silicon and achieve an increase in the readout fidelity from $(98.93\pm0.07)\,\%$ to $(99.61\pm0.04)\,\%$, while reducing threefold the overall readout time. To highlight the broader relevance of measurement-induced errors, we study a ten-dimensional ^{73}Ge nuclear spin read out through Pauli spin blockade, revealing nuclear spin flips arising from hyperfine and quadrupole interactions. We discuss the applicability of our method to other quantum hardware platforms such as color centers in diamond, spins in lithographic quantum dots, clusters of donors in silicon, and dual-species neutral atom arrays. These results unveil the effect of nonideal QND readout across diverse platforms and introduce an efficient readout protocol that can be implemented with minimal field-programmable gate array (FPGA) logic on existing hardware.

DOI: 10.1103/jtn1-wzyl

I. INTRODUCTION

Quantum error correction (QEC) [1] requires high-fidelity measurements to reliably extract error syndromes. Quantum nondemolition (QND) measurements [2] provide a powerful approach in this context because they allow repeated readout (RR) to improve confidence in the measured observable without risking changes to the underlying state. Nondemolition does not imply the absence of measurement backaction—indeed, any projective measurement inevitably collapses the wave function onto an eigenstate of the measurement operator. However, in the ideal QND case, this backaction does not accumulate when the measurement is repeated, and the system remains in the same eigenstate it was projected onto after the first shot. This principle underpins stabilizer measurements in QEC and allows for multiple cycles of error correction [3,4].

A measurement is perfectly QND if the eigenstates of the measurement operator are identical to the eigenstates of the system Hamiltonian. In ancilla-mediated QND readout, this condition is met when the system Hamiltonian H_S commutes with the Hamiltonian describing the coupling to the ancilla H_C [2,5,6],

$$[H_C, H_S] = 0. \tag{1}$$

If this condition is not met, however, the coupling to the ancilla causes a change in eigenbasis of the quantum system. The basis mismatch between the bare system and the coupled system is what we refer to as nonideal QND behavior and causes transitions between eigenstates upon repeated measurement of the quantum state.

We focus here on the case where QND readout of a quantum system is achieved by coupling it to an ancilla,

*Contact author: a.morello@unsw.edu.au

Published by the American Physical Society under the terms of the Creative Commons Attribution 4.0 International license. Further distribution of this work must maintain attribution to the author(s) and the published article's title, journal citation, and DOI.

which is subsequently and separately measured. This scenario has been employed in several platforms such as spin qubits in gate-defined quantum dots [7,8], NV center spins in diamond [9–11], trapped ions [12], neutral atoms [13], and nuclear spins [14–22]. In the case of nuclear spin qubits (with nuclear spin $I = 1/2$, Hilbert space dimension $D = 2$) [15,18] or qudits ($I \geq 1$, $D > 2$) [14,16,17,19], the ancilla is formed by a hyperfine-coupled electron. The nuclear spin measurement proceeds by first making the electron spin state depend on the nuclear one—usually via a selective spin-inversion pulse—and then reading out the electron ancilla. For the case where readout is performed electrically, the electron is spin-dependently [23–25] allowed to tunnel to the island of a single electron transistor (SET) [15,25,26], or to a nearby quantum dot (QD) [27], or through a spin-polarized scanning tunneling microscope tip [19]. Upon tunneling, the coupling Hamiltonian formed by the hyperfine interaction suddenly decreases to zero, which perturbs the eigenstates of the nuclear spin. As a result, the nuclear state will be projected onto a slightly modified eigenbasis which probabilistically causes the nuclear spin to flip. This effect is known as ionization shock [15,28,29]. It is usually possible to quantify the deviation from ideal QND measurement by counting, on average, how many electron ionization events are necessary to induce an accidental flip of the nuclear state [15,29].

In this work, we demonstrate an adaptive readout protocol that improves the QND readout fidelity of a $D = 8$ nuclear qudit by minimizing the number of electron ionization events. Instead of performing repeated QND readout cycles over the full D-dimensional state space of a quantum system, after a single successful readout event the protocol adaptively switches to measuring the remaining $D - 1$ states, which we refer to as the "dark-state subspace." The electron spin readout is a type of "negative-result measurement" [30], where one of the outcomes is associated with the absence of tunneling [31]. Therefore, probing the dark-state subspace allows the extraction of information without paying the penalty of measurement-induced spin flips. In the ideal limit of perfect ancilla readout, a negative measurement outcome within the dark-state subspace is truly QND, because the Hamiltonian remains unchanged throughout the process. Using the adaptive readout protocol, we report an increase in the average readout fidelity from $(98.93 \pm 0.07)\,\%$ to $(99.61 \pm 0.04)\,\%$, compared to regular repeated QND readout, while achieving a factor 3 speedup.

II. CONDITIONS FOR AN ADVANTAGE WITH THE ADAPTIVE READOUT PROTOCOL

We establish four necessary conditions under which the adaptive QND readout protocol would be beneficial.

(1) **Indirect readout via an ancilla.** The state of a data qubit or qudit is read out indirectly via a coupled ancilla, allowing for repeated measurements of the data system through the ancilla.

(2) **Noncommuting system-ancilla coupling.** The coupling Hamiltonian between the data system and the ancilla does not commute with the intrinsic Hamiltonian of the data system: $[H_S, H_C] \neq 0$. Changing the coupling Hamiltonian during readout thus leads to a change in the system's eigenbasis, which can induce probabilistic state transitions. Usually, one will seek the noncommutative nature of the coupling to be small, otherwise the measurement is too drastically non-QND.

(3) **Measurement changes the system dynamics.** The act of measuring the ancilla modifies its interaction with the data system. This includes both coherent (Hamiltonian) changes and dissipative (Lindblad operators) changes.

(4) **Outcome-dependent QND-ness (generalized negative-result measurement).** The measurement-induced transitions on the data system depend on the ancilla measurement outcome. In the limiting case, one outcome corresponds to a negative-result measurement and is perfectly QND, while the other induces a perturbation in the system. Generally, the protocol is beneficial whenever different measurement outcomes lead to different degrees of non-QND backaction, even if none of the outcomes are fully QND.

First, we show that all four conditions are satisfied for the ^{123}Sb nuclear spin studied here. Then, we demonstrate the performance gain of adaptive readout compared to conventional repeated QND on this platform. Finally, we discuss alternative quantum computing platforms where these conditions hold and where the adaptive readout protocol presented here could be similarly advantageous.

III. METHODS

We demonstrate the adaptive readout protocol on a quadrupolar spin-7/2 ^{123}Sb nucleus implanted in isotopically enriched silicon, forming an eight-dimensional qudit [16,17]. A hyperfine-coupled electron acts as an ancilla for QND readout and is tunnel-coupled to a nearby charge reservoir [condition 1, see Fig. 1(a)]. The measurement-induced dynamics of the system is governed by the Hamiltonians of the qudit, the ancilla, and their coupling, which we describe below.

A. System Hamiltonian and measurement-induced dynamics

In the presence of a magnetic field B_0, the ^{123}Sb donor is described by the Hamiltonian

$$H = H_S + H_A + H_C. \tag{2}$$

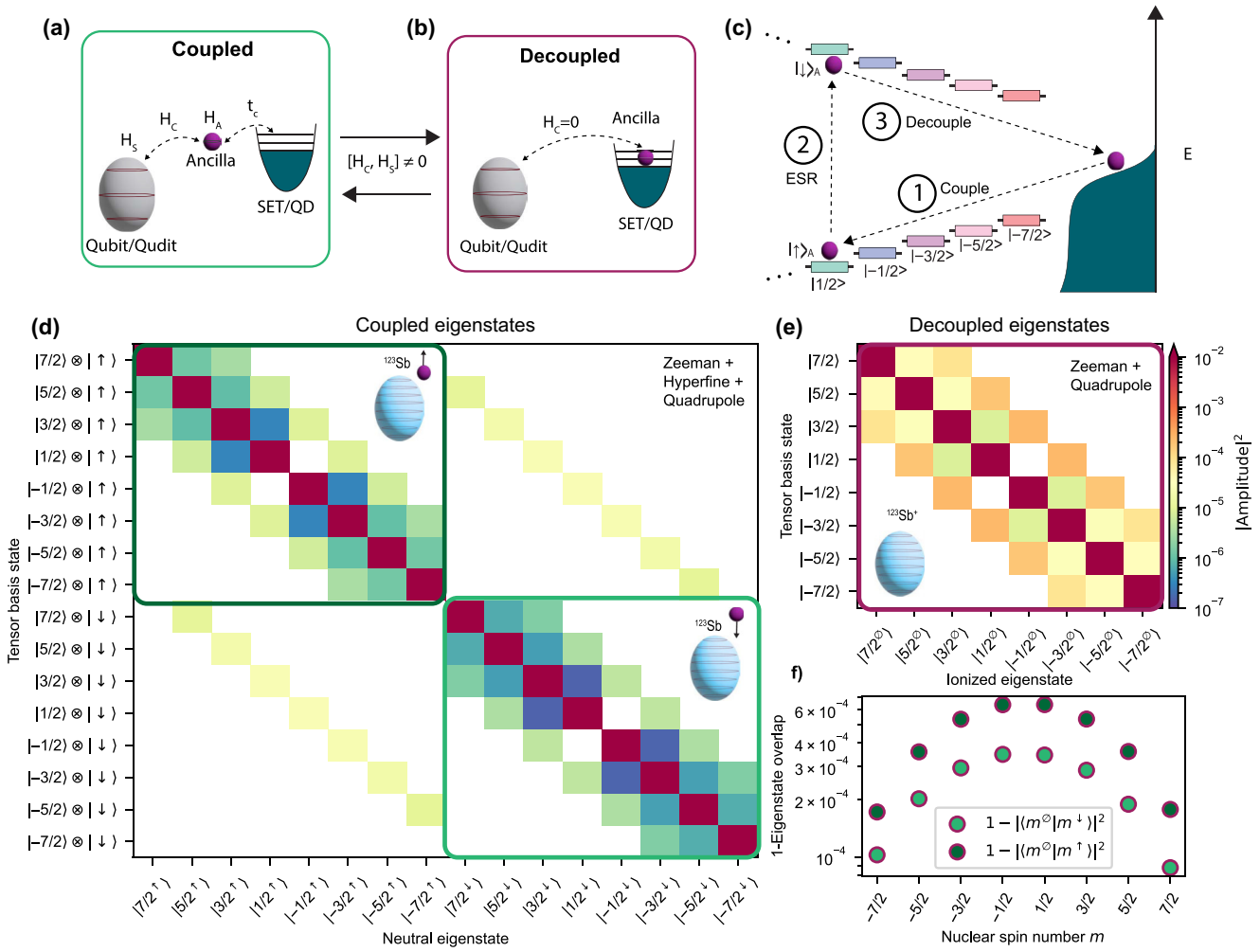


FIG. 1. Deviation from ideal quantum nondemolition measurements due to an eigenbasis mismatch of coupled and decoupled systems. (a) In the coupled system, the qubit or qudit is coupled to an ancilla, which is tunnel-coupled to a reservoir or quantum dot. (b) If the ancilla tunnels onto the reservoir or quantum dot, the coupling Hamiltonian H_c reduces to 0. This process induces spin flips if $[H_S, H_C] \neq 0$. (c) One quantum nondemolition cycle consists of coupling, conditional electron spin resonance, and decoupling the ancilla. (d) The eigenstates of the coupled Hamiltonian do not fully overlap with the tensor basis due to the quadrupole and hyperfine interaction. The quadrupole shows up as $\Delta m = \pm 1, 2$ off-diagonal elements in this matrix, whereas the hyperfine enables coupling between nuclear spin $\Delta m = \pm 1$ and electron spin $\Delta m_e = \mp 1$ components, visible as off-diagonal elements in the top left and bottom right quadrants. (e) In the decoupled case, the hyperfine interaction reduces to zero ($H_C = 0$) and the influence of the quadruople becomes more pronounced. (f) The overlap of decoupled and coupled eigenstates - $|m^{\emptyset}\rangle$ and $|m^{\updownarrow}\rangle$, respectively—when the ancilla spin state is $|\downarrow\rangle$ (light green) or $|\uparrow\rangle$ (dark green).

Here, the Hamiltonian of the qudit system and ancilla are given by

$$H_S = -\gamma_n B_0 I_z + \sum_{\alpha,\beta} Q^{+}_{\alpha\beta} I_\alpha I_\beta, \tag{3}$$

$$H_A = \gamma_e B_0 S_z, \tag{4}$$

and the hyperfine coupling is defined as

$$H_C = A\vec{I} \cdot \vec{S}. \tag{5}$$

The definitions of the Hamiltonian parameters are summarized in Table I.

Equation (5) clarifies the origin of measurement-induced spin flips in the ^{123}Sb system. The hyperfine coupling Hamiltonian does not commute with either the Zeeman term (I_z) or with the quadrupolar terms ($I_\alpha I_\beta$) in H_S (condition 2). As a result, we experience a change in eigenstates upon coupling and decoupling the ancilla during QND readout (condition 3). Importantly, this change is measurement outcome-dependent: only the $|\uparrow\rangle$-outcome causes tunneling of the ancilla (condition 4). Due to the presence of both linear and quadratic spin operators, both

TABLE I. Physical parameters and operators in the system. Note that we have absorbed the physically negative sign of γ_e into the definition of the electron spin Hamiltonian, Eq. (4). The quadrupole parameters are characterized in Supplemental Material Section 1 A [32].

Symbol	Description
$B_0 = 1.395\,\mathrm{T}$	External magnetic field
$\gamma_n = 5.55\,\mathrm{MHz/T}$	Nuclear gyromagnetic ratio
$\gamma_e = 28.02\,\mathrm{GHz/T}$	Electron gyromagnetic ratio
$A = 97.5\,\mathrm{MHz}$	Hyperfine interaction
$I = [I_x, I_y, I_z]$	Nuclear spin-7/2 operators (8×8)
$S = [S_x, S_y, S_z]$	Electron spin-1/2 operators (2×2)
α, β	Cartesian indices: x, y, z
$Q^{+}_{\alpha\beta} \in [-30.48, 7.50]$ kHz	Quadrupole tensor element in the decoupled (ionized) case

first-order ($\Delta m = \pm 1$) and second-order ($\Delta m = \pm 2$) transitions will be present during QND readout, where Δm indicates the change in nuclear spin number.

B. QND readout cycle

Figure 1(d) outlines the steps of a QND readout cycle for the ^{123}Sb qudit (see also Supplemental Methods 1 of Ref. [33]). The ancilla electron is denoted by the spin states $|\uparrow\rangle$ or $|\downarrow\rangle$ when coupled to the nucleus, and $|\emptyset\rangle$ when decoupled. The nuclear spin states are defined in the basis of the eigenstates of I_z, $\{|m\rangle\}$, with $m = 7/2, 5/2, \ldots, -7/2$.

In Step 1, we induce the transition $|\emptyset\rangle \rightarrow |\downarrow\rangle$. An electron is loaded onto the nucleus from a nearby SET by applying a pulse in local gate voltages [25]. We ensure that the loaded electron is truly in the $|\downarrow\rangle$ state with high fidelity by using a *Bayesian Maxwell's demon* approach, introduced in Ref. [34].

In Step 2, we adiabatically flip the spin of the electron $|\downarrow\rangle \rightarrow |\uparrow\rangle$, conditional on the nuclear spin state using an adiabatic electron spin resonance (aESR) pulse [35], consisting of a frequency chirp that envelops the desired resonance frequency. This can be either a single selective pulse or a multifrequency pulse targeting a specific nuclear subspace [36].

In Step 3, if the aESR pulse flipped the spin to $|\uparrow\rangle$, the electron is allowed to decouple from the nucleus and tunnel back onto the SET, i.e., $|\uparrow\rangle \rightarrow |\emptyset\rangle$. The positively charged donor left behind after the electron tunnel event will switch the bias point of the SET from Coulomb blockade (SET current $I_{\mathrm{SET}} \approx 0$) to the top of a conductance peak ($I_{\mathrm{SET}} \approx 1$ nA). The current remains high until another electron, in the $|\downarrow\rangle$ state, tunnels back onto the SET. If this current blip exceeds a threshold, the electron spin state is labeled as $|\uparrow\rangle$ [25].

To determine the nuclear spin state, we repeatedly cycle through the eight ESR resonance frequencies (Step 2). From the resulting set of tunnel events, we assign a $|\uparrow\rangle$-probability to each nuclear state and assign the nuclear state as the one with the highest $|\uparrow\rangle$ probability.

C. Eigenstate overlap

We model nuclear spin-flip probabilities by calculating overlaps between the eigenstates of the coupled (neutral donor) and decoupled (ionized donor) Hamiltonians. We label the eigenstates of the coupled system $|m^{\updownarrow}\rangle$, where m is the dominant nuclear spin projection in each specific eigenstate. In general $|m^{\updownarrow}\rangle \neq |m\rangle \otimes |\updownarrow\rangle$, because the terms contained in the hyperfine and quadrupole Hamiltonians do not commute with I_z. Similarly, the eigenstates of the decoupled system, $|m^{\emptyset}\rangle$ do not coincide with the $|m\rangle$ basis states because of the quadrupole interaction. In Fig. 1(d) we then plot the overlap of the coupled eigenstates with the tensor product states $|m\rangle \otimes |\updownarrow\rangle$, and in Fig. 1(e) the overlap of the decoupled eigenstates with the $|m\rangle$ basis states [6,37].

In the coupled case, both hyperfine and quadrupole interactions contribute to the eigenstate composition. The hyperfine term introduces "flip-flop" mixing of electron and nuclear spin components [38]; i.e., the $|5/2^{\uparrow}\rangle$ eigenstate includes a small admixture of the $|7/2\rangle \otimes |\downarrow\rangle$ basis state [top right and bottom left quadrant of Fig. 1(d)]. The quadrupole interaction adds mixing between nuclear spin states, visible as both first and second off-diagonal elements in Fig. 1(c), since the quadrupolar interaction contains quadratic terms in the spin operators (e.g., I_x^2, I_y^2). Overall, the presence of the vastly dominant electron Zeeman term ($\sim$40 GHz here) and the associated $I_z S_z$ hyperfine coupling ($\sim$100 MHz) ensure that the coupled eigenstates remain quite close to the tensor product basis, with cross-couplings well below 10^{-4}.

The eigenstates of the decoupled system [Fig. 1(e)] show stronger nuclear mixing, since the quadrupole interaction ($\sim$20 kHz) is no longer overwhelmed by the $I_z S_z$ term in the hyperfine coupling, and only competes with the nuclear Zeeman energy ($\sim$8 MHz). As a consequence, the overlap between coupled and decoupled eigenstates is imperfect.

Figure 1(f) shows that the overlap with the ionized eigenstates $|m^{\emptyset}\rangle$ is larger for the $|m^{\downarrow}\rangle$ states compared to the $|m^{\uparrow}\rangle$ states. This can be understood as follows. In the ionized case, the nuclear spin is subjected solely to the magnetic field B_0, oriented along $+z$. In the neutral case, it is also subjected to an effective hyperfine field that, due to the negative value of γ_e, points opposite to the electron spin orientation. The hyperfine coupling $A \approx 100$ MHz is much larger than the nuclear Zeeman term ≈ 8 MHz, which means that the effective field applied to the nucleus flips to $-z$ when the electron is $|\uparrow\rangle$. Transverse quadrupole terms such as I_x^2, I_y^2 then mix the nuclear eigenstates $|m\rangle$ with $|m \pm 2\rangle$, and the sign flip of the effective field in the

$|\uparrow\rangle$ case inverts the relative phase of this admixture (see Supplemental Material Section I C [32]). Therefore, the decoupling process $|\uparrow\rangle \rightarrow |\emptyset\rangle$ produces a stronger perturbation of the nuclear eigenstates than the coupling process $|\emptyset\rangle \rightarrow |\downarrow\rangle$.

IV. RESULTS

A. Jump trace statistics

To quantify the measurement-induced dynamics on the ^{123}Sb nucleus, we perform a simple repeated readout sequence over all eight nuclear states, as shown in Fig. 2(a). Figure 2(b) shows an example of raw measurement data, displaying an example of nuclear spin jumps of both $\Delta m = \pm 1$ and $\Delta m = \pm 2$. Due to ancilla readout imperfections, we observe both dark counts (false positives) and false negatives, which we filter out by applying a kernel-5 majority vote filter, which assigns the nuclear state as the one with the most counts in a window of five shots (see Supplemental Material Section I E [32]).

By analyzing the nuclear jump traces, we extract a transition matrix shown in Fig. 2(c), which quantifies the nuclear spin-flip probabilities during readout. We observe two important features. First, $\Delta m = \pm 2$ transitions dominate over $\Delta m = \pm 1$. This means that terms quadratic in the spin operators, i.e., the quadrupole interaction terms, have a dominant effect. Second, the flip probability is strongly state dependent, with states at the edges of the Hilbert space ($m = \pm 7/2$) being more resilient against spin flips than states in the middle ($m = \pm 1/2$).

We can qualitatively reproduce the state dependence and dominance of $\Delta m = \pm 2$ quadrupolar jumps [Fig. 2(d)] by filling in the Hamiltonian parameters found in Eqs. (2)–(5), calculating the eigenstates and computing the transition matrix in Eq. (S9).

Our model excludes both flip-flop-mediated relaxation and phonon-mediated nuclear T_1 processes, which are negligible on the measurement timescales. Strong flip-flop relaxation, which couples $|m_I\rangle|\downarrow\rangle \leftrightarrow |m_I - 1\rangle|\uparrow\rangle$ states, would lead to asymmetries in the measured transition matrix in Fig. 2(c). Because the electron spin is predominantly in the $|\downarrow\rangle$ state during readout, flip-flop relaxation would preferentially lower the nuclear spin eigenstate $|m_I\rangle \rightarrow |m_I - 1\rangle$. The absence of such asymmetries in the experimental data provides evidence that flip-flop relaxation is negligible under our conditions. Direct phonon-mediated spin relaxation is expected to be orders of magnitude longer than flip-flop relaxation [38], and therefore does not significantly contribute.

The jump traces additionally provide the ancilla readout confusion matrix, including the dark-count probability (false positive) and probability of missing a count (false negative), which we feed into our readout model in the next section.

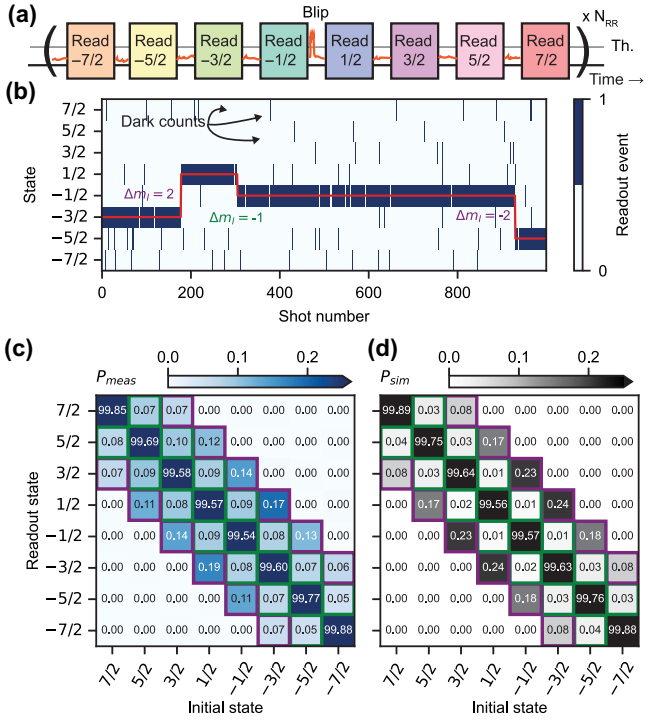


FIG. 2. Characterization of measurement-induced nuclear spin flips in ^{123}Sb. (a) Pulse sequence to probe measurement-induced dynamics. We sequentially perform quantum nondemolition readout of the nuclear states $|-7/2\rangle$ through $|+7/2\rangle$, repeated N_{RR} times. The nuclear state is detected by a short blip of current, caused by the ancillary electron tunneling to a nearby single electron transistor. If the blip exceeds the threshold, we count it as a readout event. (b) Raw readout results. We determine the most likely state (red line) by window filtering the raw data, to exclude dark counts. We observe the nucleus jumping by either $\Delta m = \pm 2$ (purple) or $\Delta m = \pm 1$ (green). The acquisition time of 1000 nuclear shots in this experiment is 43.4 s. (c) Extracted transition probability matrix, averaged over 64 000 shots. The first and second off-diagonal entries (green and purple) correspond to $\Delta m = 1$ and $\Delta m = 2$ jumps, respectively. (d) Simulated transition probability matrix based on eigenstate overlap of the coupled and decoupled nucleus. See Supplemental Material Section I for model details [32].

B. Adaptive readout protocol

In an ideal QND measurement, increasing the readout repetitions would lead to better readout fidelity. In the presence of deviations from QND ideality, however, each measurement shot poses the risk of altering the measured state. The two phenomena lead to a trade-off whereby the readout fidelity will reach a maximum as a function of measurement shots, before deteriorating due to QND nonideality.

To mitigate this undesirable trade-off, we implement an adaptive QND readout protocol that minimizes the impact of QND nonideality. Contrary to the conventional repeated QND readout approach [Fig. 3(a)], the adaptive

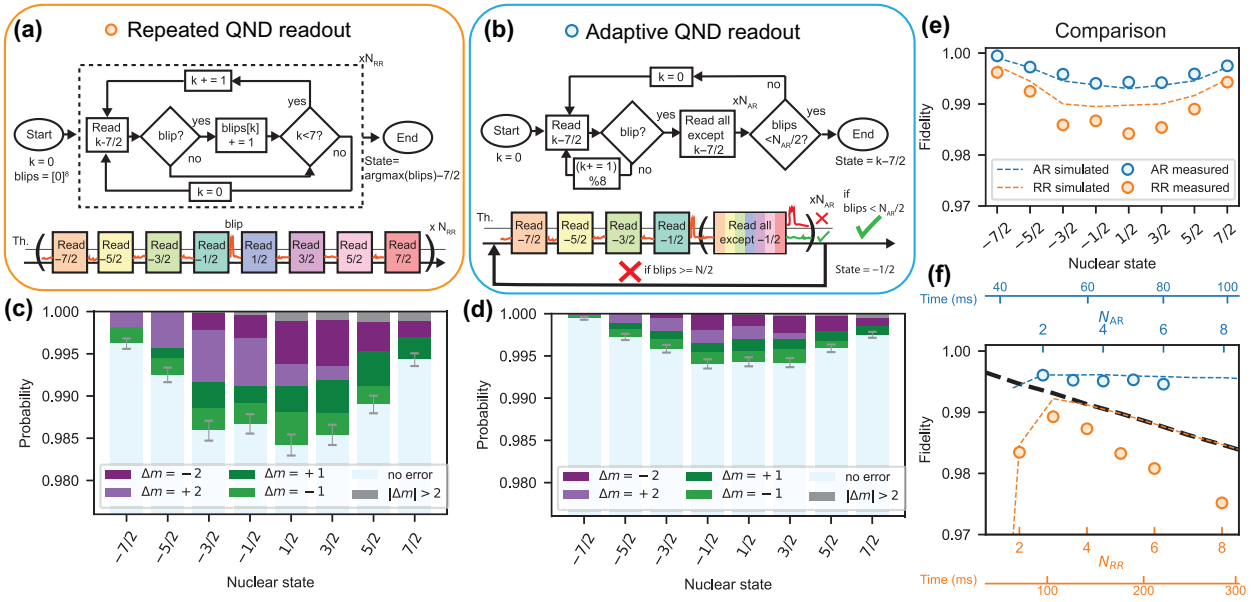


FIG. 3. Readout improvement using an adaptive quantum nondemolition protocol. (a) Decision tree of conventional repeated readout and corresponding pulse sequence. k indicates the index of nuclear state $|m\rangle = |k - 7/2\rangle$. (b) Decision tree of the adaptive readout protocol and an example of a corresponding pulse sequence. As soon as a readout event is detected, the protocol switches to measuring the dark-state space N_{AR} times. (c) Nuclear flip probabilities obtained from 10 000 repetitions of repeated readout using an optimal number of shots $N_{\mathrm{RR}} = 3$. We attribute $|\Delta m| > 2$ errors to dark counts, which are not filtered out when benchmarking the readout fidelity. The probability of such dark-count–induced errors increases for states measured later in the array, since in the case of equal counts the state is assigned to the first index. The error bar on the "no error" (light blue) datapoint indicates the 1σ confidence interval. (d) Nuclear flip probabilities over 20 000 repetitions of adaptive readout with an optimal number of dark subspace shots $N_{\mathrm{AR}} = 2$. The adaptive protocol reduces $\Delta m = 1$ (green) and $\Delta m = 2$ (purple) transition probabilities. (e) Comparison of adaptive readout (blue) and repeated readout (orange), simulated (lines) and data (dots). The adaptive readout data approach the ionization shock limit for one shot. (f) Average readout fidelity comparison vs number of readout shots and vs time for repeated readout (orange, bottom axis) and adaptive readout (blue, top axis). The black dashed line indicates the simulated repeated readout fidelity if the readout is solely limited by ionization shock (i.e., in the limit of perfect ancilla readout). Note that the blue time axis is slightly nonlinear due to the variable amount of resets of the adaptive protocol. The error bars in (e) and (f) are smaller than the markers.

protocol increases the readout fidelity without the added cost of increasing the amount of Hamiltonian-perturbing tunneling events.

The protocol is executed in two subroutines [Fig. 3(b)]. In the first subroutine, we read each nuclear state sequentially until one tunneling event (blip) is detected. The nuclear state associated with this blip is our initial guess. In the second subroutine, instead of repeating QND cycles over all nuclear states—risking multiple tunneling events—we perform a collective measurement of the entire nuclear subspace *excluding* the initial guess. We call this the *dark-state subspace*. The collective measurement is implemented by applying seven ESR pulses while the electron stays coupled—one for each state in the dark-state subspace—and only then pulsing the SET to allow for a possible tunnel event. Thus, the dark subspace readout effectively probes all remaining nuclear states in a single wait time, eliminating the need to wait separately for each of the eight states, which is a key advantage of the adaptive protocol.

In case the initial guess was correct, tunneling events should be absent in the dark-state subspace measurement. By setting a tunneling event threshold—here we choose $\mathrm{th} = \lceil N_{\mathrm{AR}}/2 \rceil$, where N_{AR} is the number of dark subspace readout shots—we decide whether we accept the initial guess (if $N_{\mathrm{blips}} < \mathrm{th}$) or reject it. As soon as $N_{\mathrm{blips}} \geq \mathrm{th}$, we discard the initial guess, cut the second subroutine, and repeat the protocol.

This strategy allows us to identify the nuclear state with, in principle, just a single electron tunneling event per nuclear spin readout, which significantly reduces measurement-induced spin flips compared to repeated QND readout. The results displayed in Figs. 3(c) and 3(d) confirm the improvement in readout with the adaptive protocol. When we apply the adaptive protocol, we observe a clear reduction in both the $\Delta m = 1$ (green) and $\Delta m = 2$ (purple) transition probabilities, consistent with a reduction in the number of tunneling events that occurred throughout the protocol. We also see a reduction of $|\Delta m| > 2$ errors

TABLE II. Confusion matrix for ancilla (electron spin) readout in the ^{123}Sb system.

TP $= 96.8 \pm 0.3\,\%$	FN $= 3.2 \pm 0.3\,\%$
FP $= 1.9 \pm 0.1\,\%$	TN $= 98.1 \pm 0.1\,\%$

[gray bars in Fig. 3(c)], which we attribute to dark counts.

Figure 3(e) shows a comparison between repeated readout (RR) and adaptive readout (AR), both with an optimized number of readout shots N_{RR} and N_{AR}. We show that the AR fidelities are on par with the measured single-shot ionization shock probabilities [from Fig. 2(c)]; the optimal data point at $N_{\mathrm{AR}} = 2$ coincides with the y-intercept of the black dashed line, confirming that the AR protocol indeed requires approximately only one tunneling event. Furthermore, the measured readout fidelities for the adaptive protocol in Figs. 3(e) and 3(f) are consistent with the simulated ones described in Sec. IV C, which takes into account imperfect ancilla readout (Table II). The deviation from the simulation observed for RR can likely be attributed to day-to-day variations in the quadrupole tensor or the ancilla readout fidelity, which leads to differences in the transition matrix compared to Fig. 2(c) and variations in the number of tunneling events due to dark counts.

In addition to achieving better readout fidelities, the AR protocol provides a threefold speedup compared to the repeated QND readout. In the AR protocol, detecting the first blip takes on average four shots, followed by dark subspace readout with $N_{\mathrm{AR}} = 2$. Since the initial guess is rejected approximately 13% of the time, the total average number of QND cycles of $\langle N_{\mathrm{QND}}\rangle_{\mathrm{AR}} = 1/(1-0.13) \times 6 \approx 6.9$.

In contrast, the RR protocol requires $N_{\mathrm{RR}} = 3$ [Fig. 3(f), orange dots] repeated over eight states, giving $\langle N_{\mathrm{QND}}\rangle_{\mathrm{RR}} = 3 \times 8 = 24$ QND cycles. Accounting for the longer dark subspace pulse duration in the AR sequence, the AR protocol achieves an effective speedup of about a factor of 3.

C. Simulations with imperfect ancilla readout

In our experiments, the ancilla readout fidelity is already high with a true-positive probability of 0.968 ± 0.003 and a false-positive probability of 0.019 ± 0.001—extracted from the raw traces of Fig. 2. To verify the robustness of the AR protocol under less ideal ancilla readout conditions, we perform a Monte-Carlo simulation of both the RR and AR protocols using the experimentally obtained transition matrix (Fig. 2) as a function of the ancilla readout fidelity [39].

For the RR protocol [Fig. 4(a)] we find that a reduction in the ancilla readout fidelity requires an increase in the optimal number of shots (red line). However, as the number of shots increases, so does the probability of measurement-induced transitions due to increased exposure to tunneling events. In Fig. 4(b) we find that, after reaching a maximum, the maximum readout fidelity gradually decreases as a function of the number of shots, illustrating the trade-off between increased knowledge due to more shots and increased probability of a state transition due to nonideal QND conditions.

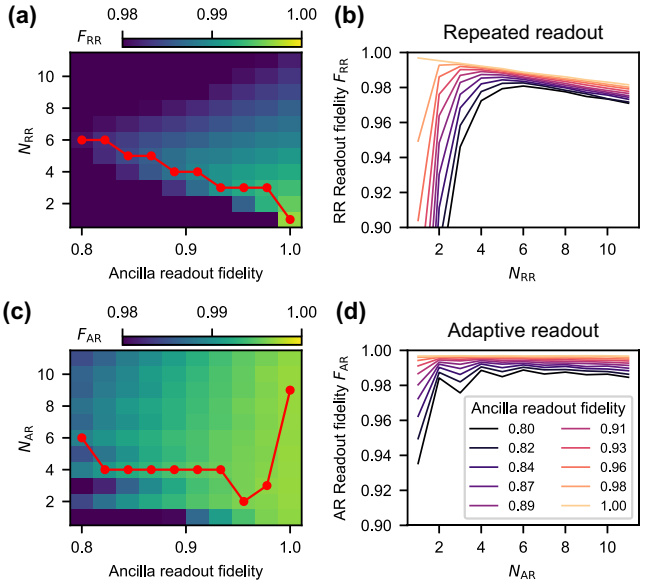


FIG. 4. Simulated comparison of repeated and adaptive readout protocols. (a) Optimal number of repeated readout shots (red line) increases as ancilla fidelity decreases. (b) Maximum fidelity in repeated readout F_{RR} decreases with shot number N_{RR} due to nonideal quantum nondemolition conditions. (c) Adaptive readout achieves higher fidelities overall compared to repeated readout. When the ancilla readout fidelity approaches 1, the adaptive readout fidelity F_{AR} becomes insensitive to the number of shots N_{AR} due to the lack of tunneling events. The simulated optimal number of shots in that regime (red line) is subject to numerical fluctuations. (d) Adaptive readout fidelity remains robust against increasing dark space shots N_{AR}, confirming suppression of measurement-induced errors. We ascribe oscillations in even-odd number of shots to the definition of the threshold th $= \lceil N_{\mathrm{AR}}/2 \rceil$, which slightly favors even N_{AR}.

In contrast, in the AR protocol [Fig. 4(c)], the fidelity remains relatively flat as a function of the number of dark subspace shots, confirming that the AR protocol indeed avoids measurement-induced transitions. We see overall higher readout fidelities compared to the RR case, where the fidelities are limited by the expected number of tunneling events, which increases with imperfect ancilla readout fidelity due to dark counts. A reduction in ancilla readout fidelity does slightly increase the AR protocol overhead, and in its turn, exposure to tunneling events, because incorrect initial guesses would be rejected more frequently (see Supplemental Material Section I F [32]).

V. APPLICABILITY TO OTHER SYSTEMS

To illustrate that nonideal QND conditions are a broader challenge in quantum devices, we consider alternative platforms with different readout mechanisms. Below, we briefly discuss the four necessary conditions for each platform and summarize the results in Table III.

A. Iso-electronic nuclei with Pauli spin blockade readout

We study an iso-electronic ^{73}Ge nuclear spin qudit in silicon, hyperfine-coupled to an electron in a quantum dot. Unlike the donor case, here the electron spin is measured using Pauli spin blockade (PSB) via an adjacent quantum dot [22]. Despite this different readout method, we observe measurement-induced nuclear spin-flip signatures similar to those in ^{123}Sb.

Condition 1: The nuclear spin state is read out indirectly via the hyperfine-coupled electron, which acts as an ancilla.

Condition 2: The hyperfine interaction between the electron and nucleus does not commute with the nuclear Zeeman Hamiltonian.

Condition 3: PSB readout involves electron tunneling, which abruptly changes the hyperfine Hamiltonian.

Condition 4: Measurement-induced nuclear spin flips depend on the electron parity outcome—the nontunneling outcome is preferred.

TABLE III. Summary of physical platforms satisfying the four conditions required for an advantage with the adaptive quantum nondemolition readout protocol. In all cases, the data system is read out indirectly via an ancilla whose measurement induces an outcome-dependent perturbation on the system.

Platform	Condition 1: Indirect readout	Condition 2: Noncommuting coupling	Condition 3: Measurement modifies dynamics	Condition 4: Outcome-dependent QND-ness
High-spin donor qudits, e.g., ^{123}Sb	Nuclear spin read out via hyperfine-coupled electron ancilla	Hyperfine and quadrupole terms do not commute with nuclear Zeeman Hamiltonian	Electron spin readout involves spin-dependent tunneling, modifying the coupling Hamiltonian	One ancilla outcome is destructive (tunneling), while the other preserves coupling
Iso-electronic nuclei coupled to quantum dots (PSB readout)	Nuclear spin measured via ESR of a hyperfine-coupled electron in a double quantum dot	Hyperfine interaction does not commute with nuclear Zeeman Hamiltonian	PSB is a spin-dependent tunneling process, modifying the coupling Hamiltonian	PSB results in one destructive ancilla outcome (tunneling), while the other preserves coupling.
Color centers in diamond (NV, SiV, GeV)	Nuclear spin mapped onto and read out via an electron spin ancilla	Transverse hyperfine terms do not commute with nuclear Zeeman term	Optical cycling or spin-to-charge conversion introduces stochastic electron dynamics	Bright-state readout induces significantly more nuclear spin flips than dark-state readout
Gate-defined quantum dot spin qubits	Data qubit read out via exchange-coupled ancilla spin	Transverse exchange terms do not commute with Zeeman Hamiltonian	Spin-dependent tunneling of the ancilla abruptly removes exchange coupling	One ancilla outcome is destructive (tunneling), while the other preserves coupling
(Clusters of) spin-1/2 donors in silicon	Multinuclear register read out via a shared electron ancilla	Electron hyperfine coupling to multiple nuclei does not commute with nuclear Zeeman terms	Electron tunneling during readout modifies the hyperfine interaction for all nuclei	Nuclear backaction depends on whether the electron tunnels or remains bound
Dual-species neutral atom arrays	Data qubit (Rb) is read out indirectly using a different atomic species (Cs) as an ancilla	Rydberg-mediated dipole-dipole interactions do not preserve the ground-state hyperfine eigenbasis	Ancilla readout involves optical pumping and Rydberg excitation, modifying the interspecies interaction during measurement	QND-ness depends on the measurement outcome: reported probabilities $P_0^{\mathrm{QND}} = 0.97(2)$ and $P_1^{\mathrm{QND}} = 0.91(2)$ indicate asymmetric QND-ness

Figure 5(b) shows the statistics of measurement-induced spin state transitions for all ten eigenstates of the ^{73}Ge nucleus. Similar to the ^{123}Sb system, we observe both $\Delta m = \pm 1$ and $\Delta m = \pm 2$ measurement-induced nuclear spin flips. Each ESR frequency sweep produces one nuclear spin-state assignment, but it is important to note that the ESR measurement involves multiple tunneling events. Specifically, for every sweep we record 201 frequency points, and at each point the hyperfine-coupled electron is reinitialized through a tunneling-out and tunneling-in process, independent of the readout outcome. As a consequence, the system undergoes approximately $N_{\text{tunnel}} = 201$ electron tunneling cycles per sweep, each governed by a bare Markov transition matrix T_{Ge}. The transition matrix shown in Fig. 5(b) therefore represents the compounded transition probabilities of 201 tunnel events, i.e., T_{Ge} raised to the power $N_{\text{tunnel}} = 201$. To extract the transition probabilities per QND cycle, we calculate the bare Markov matrix T_{Ge} (see Supplemental Material Section II B [32]) and display the spin-flip probability per shot in Figs. 5(c) and 5(d).

We demonstrate a clear reduction of the transition probabilities for jumps of both $\Delta m = \pm 1$ (green) and $\Delta m = \pm 2$ (purple) from $B_0 = 0.3$ T (light colors) to $B_0 = 1$ T (dark colors). The reduction of spin flips with an increased magnetic field can be explained by the eigenstate overlap of the coupled and decoupled qudit. If the magnetic field is increased, the relative energies of the hyperfine and quadrupole interactions are reduced with respect to the Zeeman energy. As a consequence, eigenstates are more polarized along the magnetic field direction at high magnetic fields, and the overlap of the coupled and decoupled eigenstates is increased.

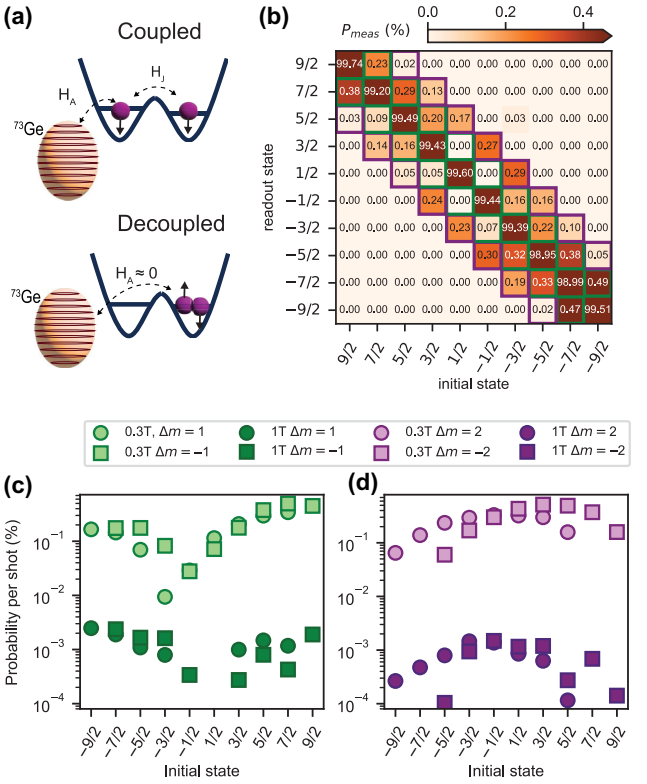


FIG. 5. Measurement-induced spin flips in a ^{73}Ge donor coupled to a double quantum dot. (a) Schematic of the system. (b) Measurement-induced nuclear spin transition matrix for one electron spin resonance spectroscopy frequency sweep of 201 points. The transition matrix shows primarily $\Delta m = 1$ (green) and $\Delta m = 2$ (purple) jumps, similar to backaction dynamics seen in the ^{123}Sb system. (c) and (d) Estimated transition probabilities per quantum nondemolition cycle. Increasing the magnetic field from $B_0 = 0.3$ T (light) to $B_0 = 1$ T (dark) reduces the transition probabilities.

B. Color centers in diamond

Color centers in diamond, such as NV^-, SiV^-, or GeV^- centers, are known to suffer from measurement-induced spin flips when nuclear spins are read out via an electron ancilla. Notably, NV centers have recently demonstrated fault-tolerant operations of logical qubits [11]. Measurement-induced errors in NV centers have been recognized since early single-defect experiments [9]. In particular, Robledo *et al.* [10] observed a decay of the QND readout fidelity under repeated measurements.

Condition 1: In NV centers, the nuclear spin is mapped onto a hyperfine-coupled electron spin, which is subsequently read out optically.

Condition 2: The coupling between a nucleus and the electron ancilla is given by: $H_c = A_{\parallel} S_z I_z + A_{\perp} S_z I_x$, where the perpendicular part does not commute with the nuclear Zeeman Hamiltonian .

Condition 3: Electron spin readout is performed by resonantly cycling a single electron spin state, typically $m_S = 0$. Optical cycling introduces stochastic transitions that change the interaction experienced by the nuclear spin during measurement.

Condition 4: Crucially, the perturbation of the nuclear spin depends on the ancilla outcome. Robledo *et al.* reported a 6% probability of a nuclear spin flip per readout cycle when the bright state is pumped. Therefore, it is preferred to read out the dark state rather than the bright state, similar to the case of a donor nucleus, where the nontunneling outcome is preferred.

C. Spin qubits in gate-defined quantum dots

A method for QND readout of a spin qubit in a gate-defined quantum dot using a neighboring ancilla spin was demonstrated in Refs. [7,8]. An exchange-coupled ancilla enables the readout of the data qubit via spin-dependent tunneling into a cold reservoir. Variants of this scheme can also be extended to Pauli Spin Blockade by using two ancilla quantum dots, similar to Fig. 5(a).

Condition 1: The state of the data qubit is mapped onto the ancilla using a conditional π-rotation.

Condition 2: The coupling Hamiltonian is given by the exchange interaction $\hat{H}_C = J\mathbf{S_1} \cdot \mathbf{S_2}$, which contains transverse terms $(\hat{S}_{1x}\hat{S}_{2x}, \hat{S}_{1y}\hat{S}_{2y})$ that do not commute with the Zeeman Hamiltonian ($H_S \propto S_{1z}$) of the individual spins.

Condition 3: During spin-to-charge readout, the spin-up ancilla state is destructively measured by tunneling, which abruptly removes the exchange coupling.

Condition 4: The spin-down ancilla state remains in the dot and continues to interact with the data qubit. As a result, the disturbance of the data qubit depends on the ancilla outcome. One measurement result is more disruptive than the other, which naturally motivates an adaptive readout strategy that favors the less disruptive spin-down outcome.

In many devices, the exchange coupling can be ramped down before readout, which would reduce measurement-induced spin flips. However, this is not always possible. Residual exchange may remain due to pulse ramping constraints [40] and in recently demonstrated always-on exchange architectures, the interaction may not be fully switched off at all [41,42].

D. (Clusters of) spin-1/2 donors in silicon

The adaptive readout protocol is also applicable to spin-1/2 donors in silicon, such as ^{31}P. Recent experiments have significantly expanded the size of donor-based nuclear spin registers. Reference [20] demonstrated an 11-qubit atomic processor composed of 4P and 5P nuclear spin clusters, while Ref. [21] report quantum error detection on a 4P nuclear spin cluster.

Condition 1: In both cases, the nuclear spin register is read out via a single electron ancilla that is hyperfine coupled to all nuclei in the cluster.

Condition 2: The hyperfine interaction between the electron and multiple nuclei does not commute with the nuclear Zeeman Hamiltonians.

Condition 3: During electron spin readout, the electron is subject to spin-dependent tunneling, which abruptly modifies the hyperfine coupling experienced by the nuclear register.

Condition 4: As in the single-donor case, this modification depends on the electron readout outcome, leading to outcome-dependent backaction on the nuclear spins.

Reference [20] reports nuclear spin-flip probabilities per readout cycle of 0.08(2)% and 0.09(1)% for the 4P and 5P registers, respectively, and note that repeated readout leads to a degradation in fidelity due to accumulated nuclear spin flips. In such multiqubit registers, the adaptive protocol can reduce the impact of these nonideal QND conditions by conditioning on the less disruptive readout outcome (the nontunneling one).

E. Dual-species neutral atom arrays

In Ref. [13], Anand *et al.* demonstrated the operation and mid-circuit QND readout in a dual-species Rydberg atom array.

Condition 1: The repeated QND readout of rubidium atoms is performed by using cesium atoms as ancilla.

Condition 2: During readout, population is transferred to Rydberg states where dipole-dipole interactions act on electronic degrees of freedom that do not preserve the ground-state hyperfine eigenbasis, such that the effective interaction Hamiltonian does not commute with the qubit Hamiltonian.

Condition 3: Upon readout, similar to NV-center optical readout, one ancilla state undergoes optical pumping which changes the interaction between the two Rydberg species.

Condition 4: Importantly, there is an asymmetry in the "QND-ness" depending on the measurement outcome. Anand *et al.* report a QND-ness probability, i.e., the probability the data qubit does not change state, of $P_0^{\mathrm{QND}} = 0.97(2)$ and $P_1^{\mathrm{QND}} = 0.91(2)$, which they attribute to the Rb atom undergoes Rydberg excitation in the $|1\rangle$ state. This QND asymmetry indicates that dual-species Rydberg arrays could benefit from using an adaptive readout scheme as well.

VI. DISCUSSION AND CONCLUSION

By adaptively minimizing tunneling events, the demonstrated readout protocol outperforms conventional repeated QND readout in both fidelity and measurement time. For the ^{123}Sb nuclear spin qudit, this adaptive approach increases the average QND readout fidelity to $99.61 \pm 0.04\,\%$. The probability of a readout error ($0.39 \pm 0.04\,\%$) nearly coincides with the single-shot ionization shock probability: $0.32 \pm 0.02\,\%$. This close correspondence indicates that the adaptive readout protocol is effectively maximally QND, achieving single-shot level disturbance, while still accumulating the information equivalent of a multishot measurement.

These improvements make it a timely resource to improve the performance and fault tolerance [43] of QEC methods where a logical qubit is encoded in the large Hilbert space of a nuclear qudit [36,44–46]. Recent work by Yu *et al.* [36] demonstrated that the ^{123}Sb nucleus can be used to encode a logical qubit in the spin-cat states of the form $|\psi_{\mathrm{cat}}\rangle_\Theta = 1/\sqrt{2}(|-7/2\rangle_\Theta + |7/2\rangle_\Theta)$, i.e., two maximally separated basis states defined along an axis Θ in the generalized rotating frame. Fault-tolerant error correction schemes require all aspects of operating the code—gates, initialization, and syndrome extraction—to exceed the fault-tolerant threshold [43].

The adaptive protocol in this work is compatible with syndrome extraction in the spin-cat code, which relies

on reading out the symmetric subspaces $\{|-5/2\rangle, |5/2\rangle\}$, $\{|-3/2\rangle, |3/2\rangle\}$, $\{|-1/2\rangle, |1/2\rangle\}$ [45]. Here we demonstrate that we can increase the average QND readout fidelity to a level consistent with estimates of error thresholds needed for fault tolerance [47,48]. The improved readout fidelity is promising for reaching beyond the break-even regime for spin-cat codes.

The added time efficiency becomes important when considering systems that have a long measurement time compared to their dephasing time T_2. Ideally, multiple rounds of error correction must be completed before the system decoheres. In the ^{123}Sb system, the readout time (on the order of milliseconds) is still comparable to the free induction decay time T_2^* [36]. This limitation can only be partially mitigated through refocusing [49] or qudit dynamical decoupling techniques [50], which extend coherence but do not address the slow readout process. The second example, ^{73}Ge, offers a promising alternative by interfacing nuclear spins with gate-defined quantum dots, enabling PSB readout, which drastically reduces the measurement time [27] (100–200 μs) [22] and allows for low-field as well as high-temperature operation [51]. More broadly, the advantages of adaptive QND readout extend to other platforms such as NV centers in diamond, dual-species neutral-atom arrays, gate-defined quantum dots and donor clusters, where outcome-dependent measurement-induced bit flips are limitations for fault-tolerant quantum computing.

ACKNOWLEDGMENTS

The research was funded by Australian Research Council Discovery Projects (Grants No. DP210103769 and No. DP250101806) and the US Army Research Office (Contract No. W911NF-23-1-0113). A.M. acknowledges support of an Australian Research Council Laureate Fellowship (Project No. FL240100181). We acknowledge the facilities, and the scientific and technical assistance provided by the UNSW node of the Australian National Fabrication Facility (ANFF), and the Heavy Ion Accelerators (HIA) nodes at the University of Melbourne and the Australian National University. ANFF and HIA are supported by the Australian Government through the National Collaborative Research Infrastructure Strategy (NCRIS) program. Ion beam facilities employed by D.N.J. and A.M.J. were co-funded by the Australian Research Council Centre of Excellence for Quantum Computation and Communication Technology (Grant No. CE170100012). X.Y., B.W., M.R.v.B., A.V., and P.S. acknowledge support from the Sydney Quantum Academy. P.S. acknowledges support from the Baxter Charitable Foundation. The views and conclusions contained in this document are those of the authors and should not be interpreted as representing the official policies, either expressed or implied, of the Army Research Office or the U.S. Government. The U.S. Government is authorized to reproduce and distribute reprints for Government purposes notwithstanding any copyright notation herein.

A.V. performed the experiment, data analysis and readout simulations. R.Y.S. wrote the measurement code and helped with simulations. L.A.O'N. performed the quadrupole Hamiltonian simulations. P.S. and G.G. performed the ^{73}Ge experiment under supervision of A.L. and A.S.D. B.W., M.N., M.R.v.B, and X.Y. gave experimental input and helped characterizing the device. D.H. and F.E.H. fabricated the device on materials supplied by K.M.I. A.M.J., D.H., and D.N.J. performed the ion implantation. C.H.Y. performed the ^{73}Ge data analysis. A.M. supervised the project. A.V. and A.M. wrote the manuscript with input from all other authors.

A.M. is an inventor on a patent related to this work, describing the use of high-spin donor nuclei as quantum information processing elements (Applications No. AU2019227083A1, No. US16/9,75,669, and No. WO2019165494A1). A.S.D. is the CEO and a director of Diraq Pty Ltd. F.E.H., C.H.Y., A.S.D., and A.L. declare equity interest in Diraq Pty Ltd.

DATA AVAILABILITY

The data that support the findings of this article are openly available [39].

[1] Simon J. Devitt, William J. Munro, and Kae Nemoto, Quantum error correction for beginners, Rep. Progr. Phys. **76**, 076001 (2013).
[2] Vladimir B. Braginsky and F. Ya Khalili, Quantum nondemolition measurements: The route from toys to tools, Rev. Mod. Phys. **68**, 1 (1996).
[3] D. Ristè, S. Poletto, M. Z. Huang, A. Bruno, V. Vesterinen, O. P. Saira, and L. Dicarlo, Detecting bit-flip errors in a logical qubit using stabilizer measurements, Nat. Commun. **6**, 6983 (2015).
[4] J. Kelly *et al.*, State preservation by repetitive error detection in a superconducting quantum circuit, Nature **519**, 66 (2015).
[5] W. G. Unruh, Quantum nondemolition and gravity-wave detection, Phys. Rev. D **19**, 2888 (1979).
[6] Benjamin Joecker, Holly G. Stemp, Irene Fernández De Fuentes, Mark A. I. Johnson, and Andrea Morello, Error channels in quantum nondemolition measurements on spin systems, Phys. Rev. B **109**, 085302 (2024).
[7] Xiao Xue, Benjamin D'anjou, Thomas F. Watson, Daniel R. Ward, Donald E. Savage, Max G. Lagally, Mark Friesen, Susan N. Coppersmith, Mark A. Eriksson, William A. Coish, and Lieven M. K. Vandersypen, Repetitive quantum nondemolition measurement and soft decoding of a silicon spin qubit, Phys. Rev. X **10**, 021006 (2020).
[8] J. Yoneda, K. Takeda, A. Noiri, T. Nakajima, S. Li, J. Kamioka, T. Kodera, and S. Tarucha, Quantum non-demolition readout of an electron spin in silicon, Nat. Commun. **11**, 1144 (2020).

[9] Philipp Neumann, Johannes Beck, Matthias Steiner, Florian Rempp, Helmut Fedder, Philip R. Hemmer, Jörg Wrachtrup, and Fedor Jelezko, Single-shot readout of a single nuclear spin, Science **329**, 542 (2010).

[10] Lucio Robledo, Lilian Childress, Hannes Bernien, Bas Hensen, Paul F. A. Alkemade, and Ronald Hanson, High-fidelity projective readout of a solid-state spin quantum register, Nature **477**, 574 (2011).

[11] M. H. Abobeih, Y. Wang, J. Randall, S. J. H. Loenen, C. E. Bradley, M. Markham, D. J. Twitchen, B. M. Terhal, and T. H. Taminiau, Fault-tolerant operation of a logical qubit in a diamond quantum processor, Nature **606**, 884 (2022).

[12] V. Negnevitsky, M. Marinelli, K. K. Mehta, H. Y. Lo, C. Flühmann, and J. P. Home, Repeated multi-qubit readout and feedback with a mixed-species trapped-ion register, Nature **563**, 527 (2018).

[13] Shraddha Anand, Conor E. Bradley, Ryan White, Vikram Ramesh, Kevin Singh, and Hannes Bernien, A dual-species Rydberg array, Nat. Phys. **20**, 1744 (2024).

[14] Romain Vincent, Svetlana Klyatskaya, Mario Ruben, Wolfgang Wernsdorfer, and Franck Balestro, Electronic read-out of a single nuclear spin using a molecular spin transistor, Nature **488**, 357 (2012).

[15] Jarryd J. Pla, Kuan Y. Tan, Juan P. Dehollain, Wee H. Lim, John J. L. Morton, Floris A. Zwanenburg, David N. Jamieson, Andrew S. Dzurak, and Andrea Morello, High-fidelity readout and control of a nuclear spin qubit in silicon, Nature **496**, 334 (2013).

[16] Serwan Asaad, Vincent Mourik, Benjamin Joecker, Mark A. I. Johnson, Andrew D. Baczewski, Hannes R. Firgau, Mateusz T. Madzik, Vivien Schmitt, Jarryd J. Pla, Fay E. Hudson, Kohei M. Itoh, Jeffrey C. McCallum, Andrew S. Dzurak, Arne Laucht, and Andrea Morello, Coherent electrical control of a single high-spin nucleus in silicon, Nature **579**, 205 (2020).

[17] Irene Fernández de Fuentes, Tim Botzem, Mark A. I. Johnson, Arjen Vaartjes, Serwan Asaad, Vincent Mourik, Fay E. Hudson, Kohei M. Itoh, Brett C. Johnson, Alexander M. Jakob, Jeffrey C. McCallum, David N. Jamieson, Andrew S. Dzurak, and Andrea Morello, Navigating the 16-dimensional Hilbert space of a high-spin donor qudit with electric and magnetic fields, Nat. Commun. **15**, 1380 (2024).

[18] J. Reiner, Y. Chung, S. H. Misha, C. Lehner, C. Moehle, D. Poulos, S. Monir, K. J. Charde, P. Macha, L. Kranz, I. Thorvaldson, B. Thorgrimsson, D. Keith, Y. L. Hsueh, R. Rahman, S. K. Gorman, J. G. Keizer, and M. Y. Simmons, High-fidelity initialization and control of electron and nuclear spins in a four-qubit register, Nat. Nanotechnol. **19**, 605 (2024).

[19] Evert W. Stolte, Jinwon Lee, Hester G. Vennema, Rik Broekhoven, Esther Teng, Allard J. Katan, Lukas M. Veldman, Philip Willke, and Sander Otte, Single-shot readout of the nuclear spin of an on-surface atom, Nat. Commun. **16**, 7785 (2025).

[20] Hermann Edlbauer, Junliang Wang, A. M. Huq, Ian Thorvaldson, Michael Jones, A. F. M. Misha, William Pappas, Christian Moehle, Yu-Ling Hsueh, Henric Bornemann, Samuel Gorman, Yousun Chung, Joris Keizer, Ludwik Kranz, and Michelle Simmons, An 11-qubit atom processor in silicon, Nature **648**, 569 (2025).

[21] Chunhui Zhang *et al.*, Quantum error detection in a silicon quantum processor, Nat. Electron. **9**, 295 (2026).

[22] Paul Steinacker, Gauri Goenka, Rocky Yue Su, Tuomo Tanttu, Wee Han Lim, Santiago Serrano, Tim Botzem, Jesus D. Cifuentes, Shao Qi Lim, Jeffrey C. McCallum, Brett C. Johnson, Fay E. Hudson, Kok Wai Chan, Christopher C. Escott, Andre Saraiva, Chih Hwan Yang, Vincent Mourik, Andrea Morello, Andrew S. Dzurak, and Arne Laucht, Coupling a ^{73}Ge nuclear spin to an electrostatically defined quantum dot, arXiv:2510.03981.

[23] J. M. Elzerman, R. Hanson, L. H. Willems van Beveren, B. Witkamp, L. M. K. Vandersypen, and L. P. Kouwenhoven, Single-shot read-out of an individual electron spin in a quantum dot, Nature **430**, 431 (2004).

[24] M. Xiao, I. Martin, E. Yablonovitch, and H. W. Jiang, Electrical detection of the spin resonance of a single electron in a silicon field-effect transistor, Nature **430**, 435 (2004).

[25] Andrea Morello, Jarryd J. Pla, Floris A. Zwanenburg, Kok W. Chan, Kuan Y. Tan, Hans Huebl, Mikko Möttönen, Christopher D. Nugroho, Changyi Yang, Jessica A. van Donkelaar, Andrew D. C. Alves, David N. Jamieson, Christopher C. Escott, Lloyd C. L. Hollenberg, Robert G. Clark, and Andrew S. Dzurak, Single-shot readout of an electron spin in silicon, Nature **467**, 687 (2010).

[26] A. Morello, C. C. Escott, H. Huebl, L. H. Willems van Beveren, L. C. L. Hollenberg, D. N. Jamieson, A. S. Dzurak, and R. G. Clark, Architecture for high-sensitivity single-shot readout and control of the electron spin of individual donors in silicon, Phys. Rev. B: Condens. Matter Mater. Phys. **80**, 081307(R) (2009).

[27] H. Geng, M. Kiczynski, A. V. Timofeev, E. N. Osika, D. Keith, J. Rowlands, L. Kranz, R. Rahman, Y. Chung, J. G. Keizer, S. K. Gorman, and M. Y. Simmons, High-fidelity sub-microsecond single-shot electron spin readout above 3.5 K, Nat. Commun. **16**, 3382 (2025).

[28] Samuel J. Hile, Lukas Fricke, Matthew G. House, Eldad Peretz, Chin Yi Chen, Yu Wang, Matthew Broome, Samuel K. Gorman, Joris G. Keizer, Rajib Rahman, and Michelle Y. Simmons, Addressable electron spin resonance using donors and donor molecules in silicon, Sci. Adv. **4**, eaaq1459 (2018).

[29] Mateusz T. Madzik, Serwan Asaad, Akram Youssry, Benjamin Joecker, Kenneth M. Rudinger, Erik Nielsen, Kevin C. Young, Timothy J. Proctor, Andrew D. Baczewski, Arne Laucht, Vivien Schmitt, Fay E. Hudson, Kohei M. Itoh, Alexander M. Jakob, Brett C. Johnson, David N. Jamieson, Andrew S. Dzurak, Christopher Ferrie, Robin Blume-Kohout, and Andrea Morello, Precision tomography of a three-qubit donor quantum processor in silicon, Nature **601**, 348 (2022).

[30] Avshalom C. Elitzur and Lev Vaidman, Quantum mechanical interaction-free measurements, Found. Phys. **23**, 987 (1993).

[31] J. T. Muhonen, J. P. Dehollain, A. Laucht, S. Simmons, R. Kalra, F. E. Hudson, A. S. Dzurak, A. Morello, D. N. Jamieson, J. C. McCallum, and K. M. Itoh, Coherent

control via weak measurements in ^{31}P single-atom electron and nuclear spin qubits, Phys. Rev. B **98**, 155201 (2018).

[32] See the Supplemental Material http://link.aps.org/supplemental/10.1103/jtn1-wzyl for details on the quadrupole characterization, measurement-induced transition model, additional data on the number of tunneling events per QND cycle and bare Markov matrices, and the experimental setups. The Supplemental Material includes Refs. [52–57].

[33] Arjen Vaartjes, Martin Nurizzo, Lin Htoo Zaw, Benjamin Wilhelm, Xi Yu, Danielle Holmes, Daniel Schwienbacher, Anders Kringhøj, Mark R. van Blankenstein, Alexander M. Jakob, Fay E. Hudson, Kohei M. Itoh, Riley J. Murray, Robin Blume-Kohout, Namit Anand, Andrew S. Dzurak, David N. Jamieson, Valerio Scarani, and Andrea Morello, Certifying the quantumness of a nuclear spin qudit through its uniform precession, Newton **1**, 100017 (2025).

[34] Mark A. I. Johnson, Mateusz T. Mądzik, Fay E. Hudson, Kohei M. Itoh, Alexander M. Jakob, David N. Jamieson, Andrew Dzurak, and Andrea Morello, Beating the thermal limit of qubit initialization with a Bayesian Maxwell's demon, Phys. Rev. X **12**, 041008 (2022).

[35] Arne Laucht, Rachpon Kalra, Juha T. Muhonen, Juan P. Dehollain, Fahd A. Mohiyaddin, Fay Hudson, Jeffrey C. McCallum, David N. Jamieson, Andrew S. Dzurak, and Andrea Morello, High-fidelity adiabatic inversion of a ^{31}P electron spin qubit in natural silicon, Appl. Phys. Lett. **104**, 092115 (2014).

[36] Xi Yu, Benjamin Wilhelm, Danielle Holmes, Arjen Vaartjes, Daniel Schwienbacher, Martin Nurizzo, Anders Kringhøj, Mark R.van Blankenstein, Alexander M. Jakob, Pragati Gupta, Fay E. Hudson, Kohei M. Itoh, Riley J. Murray, Robin Blume-Kohout, Thaddeus D. Ladd, Namit Anand, Andrew S. Dzurak, Barry C. Sanders, David N. Jamieson, and Andrea Morello, Schrödinger cat states of a nuclear spin qudit in silicon, Nat. Phys. **21**, 362 (2025).

[37] S. Monir, E. N. Osika, S. K. Gorman, I. Thorvaldson, Y. L. Hsueh, P. Macha, L. Kranz, J. Reiner, M. Y. Simmons, and R. Rahman, Impact of measurement backaction on nuclear spin qubits in silicon, Phys. Rev. B **109**, 035157 (2024).

[38] Rostyslav Savytskyy, Tim Botzem, Irene Fernandez de Fuentes, Benjamin Joecker, Jarryd J. Pla, Fay E. Hudson, Kohei M. Itoh, Alexander M. Jakob, Brett C. Johnson, David N. Jamieson, Andrew S. Dzurak, and Andrea Morello, An electrically driven single-atom "flip-flop" qubit, Sci. Adv. **9**, eadd9408 (2023).

[39] A. Vaartjes, Maximizing the nondemolition nature of a quantum measurement via an adaptive readout protocol [data set]. Zenodo, 2026, https://zenodo.org/records/18522131.

[40] Irina Heinz, Adam R. Mills, Jason R. Petta, and Guido Burkard, Analysis and mitigation of residual exchange coupling in linear spin-qubit arrays, Phys. Rev. Res. **6**, 013153 (2024).

[41] Yun-Pil Shim and Charles Tahan, Charge-noise-insensitive gate operations for always-on, exchange-only qubits, Phys. Rev. B **93**, 121410(R) (2016).

[42] Joseph D. Broz, Jesse C. Hoke, Edwin Acuna, and Jason R. Petta, Demonstration of an always-on exchange-only spin qubit, arXiv:2508.01033.

[43] Daniel Gottesman, Quantum fault tolerance in small experiments, arXiv:1610.03507.

[44] Jonathan A. Gross, Designing codes around interactions: The case of a spin, Phys. Rev. Lett. **127**, 010504 (2021).

[45] Jonathan A. Gross, Clément Godfrin, Alexandre Blais, and Eva Dupont-Ferrier, Hardware-efficient error-correcting codes for large nuclear spins, Phys. Rev. Appl. **22**, 014006 (2024).

[46] Pragati Gupta, Arjen Vaartjes, Xi Yu, Andrea Morello, and Barry C. Sanders, Robust macroscopic Schrödinger's cat on a nucleus, Phys. Rev. Res. **6**, 013101 (2024).

[47] Ashley M. Stephens, Fault-tolerant thresholds for quantum error correction with the surface code, Phys. Rev. A **89**, 022321 (2014).

[48] Gözde Üstün, Andrea Morello, and Simon Devitt, Single-step parity check gate set for quantum error correction, Quantum Sci. Technol. **9**, 035037 (2024).

[49] Cameron Jones, Piper Wysocki, Meng Ke Feng, Gerardo A. Paz-Silva, Corey I. Ostrove, Tuomo Tanttu, Kenneth M. Rudinger, Samuel K. Bartee, Kevin Young, Fay E. Hudson, Wee Han Lim, Nikolay V. Abrosimov, Hans-Joachim Pohl, Michael L. W. Thewalt, Robin Blume-Kohout, Andrew S. Dzurak, Andre Saraiva, Arne Laucht, and Chih Hwan Yang, Mid-circuit logic executed in the qubit layer of a quantum processor, arXiv:2512.12648.

[50] Vinay Tripathi, Noah Goss, Arian Vezvaee, Long B. Nguyen, Irfan Siddiqi, and Daniel A. Lidar, Qudit dynamical decoupling on a superconducting quantum processor, Phys. Rev. Lett. **134**, 050601 (2025).

[51] Jonathan Y. Huang *et al.*, High-fidelity spin qubit operation and algorithmic initialization above 1 K, Nature **627**, 772 (2024).

[52] Laura A. O'Neill, Benjamin Joecker, Andrew D. Baczewski, and Andrea Morello, Engineering local strain for single-atom nuclear acoustic resonance in silicon, Appl. Phys. Lett. **119**, 174001 (2021).

[53] David P. Franke, Florian M. Hrubesch, Markus Künzl, Hans Werner Becker, Kohei M. Itoh, Martin Stutzmann, Felix Hoehne, Lukas Dreher, and Martin S. Brandt, Interaction of strain and nuclear spins in silicon: Quadrupolar effects on ionized donors, Phys. Rev. Lett. **115**, 057601 (2015).

[54] U. Vool, I. M. Pop, K. Sliwa, B. Abdo, C. Wang, T. Brecht, Y. Y. Gao, S. Shankar, M. Hatridge, G. Catelani, M. Mirrahimi, L. Frunzio, R. J. Schoelkopf, L. I. Glazman, and M. H. Devoret, Non-Poissonian quantum jumps of a fluxonium qubit due to quasiparticle excitations, Phys. Rev. Lett. **113**, 247001 (2014).

[55] J. J. Wesdorp, L. Grünhaupt, A. Vaartjes, M. Pita-Vidal, A. Bargerbos, L. J. Splitthoff, P. Krogstrup, B. van Heck, and G. de Lange, Dynamical polarization of the fermion parity in a nanowire Josephson junction, Phys. Rev. Lett. **131**, 117001 (2023).

[56] S. Asmussen, *Applied Probability and Queues* (Springer, New York, NY, 2003).

[57] Amanda E. Seedhouse, Tuomo Tanttu, Ross C. C. Leon, Ruichen Zhao, Kuan Yen Tan, Bas Hensen, Fay E. Hudson, Kohei M. Itoh, Jun Yoneda, Chih Hwan Yang, Andrea Morello, Arne Laucht, Susan N. Coppersmith, Andre Saraiva, and Andrew S. Dzurak, Pauli blockade in silicon quantum dots with spin-orbit control, PRX Quantum **2**, 010303 (2021).